

Ultra tough and high resilience mechanochromic fibres for real world stress detection

Received: 4 September 2024

Accepted: 25 February 2025

Published online: 06 March 2025

Yu Jin Jeong^{1,3}, Youngeun Lee^{1,3}, Taekyung Won², Ji Won Lee¹,
Youngho Eom²✉ & Dae Seok Kim¹✉

Cholesteric liquid crystal elastomer fibres gain considerable attention as promising candidates for mechanochromic smart textiles across various domains, ranging from fashion to healthcare. However, intrinsically high hysteresis of cholesteric liquid crystal elastomer during stress relaxation necessitates a time-lag between successive stimulus detections, thereby constraining the practical use in real-world systems. Here, we develop high-tough and low-hysteresis mechanochromic fibres capable of effectively detecting ultra-fast deformations at practical levels. By utilizing a thermoplastic elastomer as a core fibre and cholesteric liquid crystal elastomer as a sheath, we develop sheath-core composite fibres. The cholesteric liquid crystal elastomer sheath-core fibres preserve remarkable optical properties of cholesteric liquid crystal elastomer sheath while improving mechanical properties, including high strength (100.9 MPa), toughness (2.7×10^2 MJ m⁻³), and ultra-fast resilience (60% strain at 49.98 cm s⁻¹ strain speed) due to the thermoplastic elastomer core. We demonstrate on-demand mechanochromic fibres with tuneable moduli of thermoplastic elastomer core, expanding the fields of smart textile from single fibre to dynamic sensory environment.

Fibres that are responsive to external stimuli have applications in smart textiles, healthcare^{1–4}, environmental monitoring^{5,6}, biosensing^{7,8}, motion detection^{9–11}, and smart sports apparel¹². In particular, achieving practicality and universality in smart textiles requires immediate signal transmission through colour, sound, and tactile feedback to maximise user convenience. Mechanochromic materials^{13–16} change colour upon mechanical deformation. Hence, they have applications in human-cognition-based mechanical sensors. Fibrillation of mechanochromic materials could result in a new class of smart textiles with mechanical sensing capabilities. One example of mechanochromism is structurally coloured materials, which exhibit high stability in an external environment and tuneability^{17–20}.

However, researchers must overcome two critical hurdles to apply mechanochromic fibres as commercial-level smart sensing

textiles: (1) structural colour change with high vividness over a broad wavelength shift, and (2) high mechanical durability and low hysteresis against repeated real-time stress induced by rapid deformation. To date, most structurally coloured fibres have been fabricated by embedding inelastic nanoparticles^{21–25}. The main challenge is the incompatibility between structural functionality and mechanical resilience in structurally coloured materials. Stretching the fibre alters nanoparticle spacing, affecting colour, but this leads to a compromise between vividness and durability. Cholesteric liquid crystal elastomers (CLCEs), an emerging class of mechanochromic materials, exhibit selective structural colours owing to periodic helical ordering in self-assembled liquid crystal mesogens^{26–28}. Extensive research on the mechanochromism of CLCEs has so far been focused on films^{29,30}. To the best of our knowledge, only two studies have explored the

¹Department of Polymer Engineering, Pukyong National University, Busan, Republic of Korea. ²Department of Organic and Nano Engineering, Human-Tech Convergence Program, Hanyang University, Seoul, Republic of Korea. ³These authors contributed equally: Yu Jin Jeong, Youngeun Lee.

✉ e-mail: eomyh@hanyang.ac.kr; daeseok@pknu.ac.kr

mechanochromism of neat CLCE fibres thus far—Lagerwell et al. showed a wavelength shift of 155 nm from red to blue upon the application of 200% strain to CLCE fibres, with an ultimate strength of 17.4 MPa^{31,32}.

Notably, neat CLCE fibres are unsuitable against real-time, repeated deformation owing to their large strain hysteresis. Although neat CLCE fibres recover their original structures, their weak elasticity, so called ‘soft elasticity’³³, due to the reorientation of mesogens caused by the uniaxial strain inevitably induces a time lag during stress relaxation^{34,35}. This indicates that neat CLCE fibres lose their mechanochromic capability following repeated and rapid real-world stimuli until the time lag from the preceding stimulus has elapsed.

To overcome the above-mentioned mechanical limitations of neat CLCE fibres, in this study, we developed a sheath–core (SC) composite fibre structure using heterogeneous mechanical-functional elastomers³⁶. A commercial-grade thermoplastic elastomer (TPE)^{37–41} was adopted as the core component to impart high strength and high elasticity to the resultant CLCE (named CLCE-SC), while preserving its optical properties. The harmonic SC architecture of the CLCE-SC fibres realises stress-durable, low-hysteresis mechanochromic fibres and textiles for practical applications. The elasticity of the core fibres was fine-tuned by incorporating carbon black (CB) into the TPE core⁴² with low, medium, and high mechanical moduli, which led to different colour shifts upon applying a load. Owing to the sufficiently high volume of the TPE core, the mechanical properties of the composite fibres could be controlled by manipulating only the mechanical properties of the core elastomer. In this study, we fabricated ultra-

tough and high-resilience CLCE-SC fibres capable of stable mechanochromism under real-time, high-speed cyclic deformation and systematically analysed their mechanical and optical properties. Then, we demonstrated practical applications as smart fishing lines, safety ropes, and dynamic sensory nets.

Results

Fabrication of CLCE-SC fibres

CLCE precursors and TPE fibres of 0.8 mm in diameter were prepared (details are described in Supplementary Note 1 and Supplementary Fig. 1). Continuous surface coating and in situ cross-linking of the CLCE precursor on the TPE core fibre afforded the CLCE-SC fibres (Fig. 1a and b) in four stages (I–IV) of array transformation. The TPE fibre was dipped into the CLCE precursor chamber and passed through a conical nozzle at a rate of 3 mm s^{−1}. During the transfer of the TPE fibre, the CLCE precursor was coated by shearing to form a well-aligned CLCE sheath layer. Rheological analysis demonstrated that the enhanced viscoelasticity achieved by quenching to room temperature (25 °C) suppressed Rayleigh-Plateau instability, enabling the formation of a uniform coating layer. Furthermore, an analysis based on the precursor composition revealed that an oligomer-to-monomer ratio of 1:0.5 provided optimal process efficiency and uniform coating quality. The rheological properties of the precursor are detailed in Supplementary Note 2 and Supplementary Figs. 2 and Supplementary Fig. 3. Specifically, the transition temperature of the CLCE precursor from the isotropic to cholesteric phase (T_{IC}) to be 54 °C (Fig. 1c). Therefore, the coating chamber was

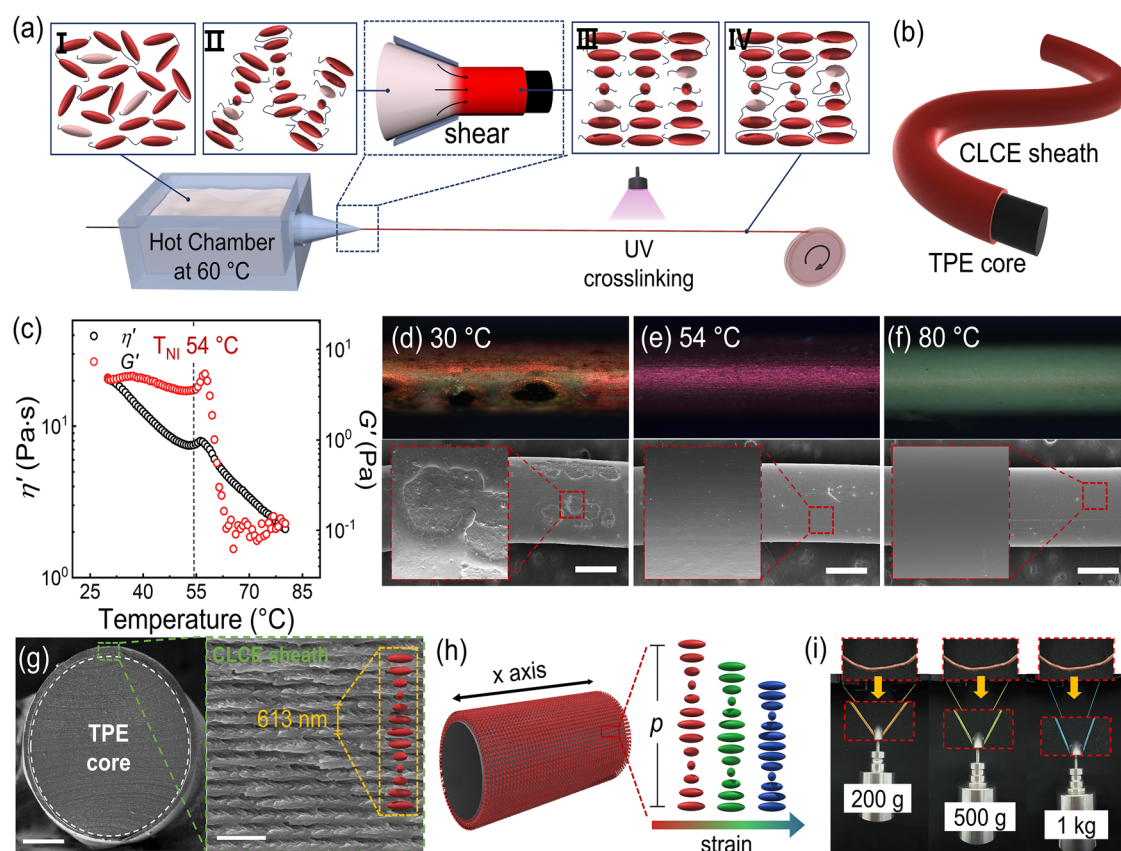


Fig. 1 | Preparation of the cholesteric liquid crystal elastomer sheath–core (CLCE-SC) fibres. **a** Schematic of the shear-coating method and molecular-level orientation changes (I–IV) during the coating process. **b** Schematic of a CLCE-SC fibre. **c** Rheological analysis to determine the isotropic–cholesteric transition temperature (T_{IC}) of the CLCE precursor. **d, e, f** Polarised optical microscopy (POM) images (top) and scanning electron microscopy (SEM) images (bottom) of a CLCE

sheath prepared at different coating temperatures. The scale bars are 500 μ m. **g** Cross-sectional SEM images of a CLCE-SC fibre (left) and the enlarged cross-section (right) showing helical pitch (p) = 613 nm. The scale bars are 200 μ m (left) and 1 μ m (right). **h** Schematic of the cholesteric structures and colour variation with pitches. **i** Photographs of the mechanochromism of the CLCE-SC fibres under different loads: 200 g, 500 g, and 1 kg.

maintained at 60 °C to maintain the CLCE precursor in the isotropic phase close to T_{IC} (Stage I). As the fibre passed through the conical nozzle, the temperature of the precursor decreased to reach a value closer to its T_{IC} (Stage II). During this transition, the mesogens were twisted by chiral dopant LC756, resulting in their self-assembly into helical structures. Subsequently, as the mesogens passed through the conical nozzle with a tip diameter of 0.9 mm, the CLCE precursor experienced shear forces that unidirectionally align the cholesteric helix (Stage III). As demonstrated in previous studies⁴³, where shear aligns short-pitch cholesteric radially, explaining the enhanced colour in cholesteric-phase coatings, our CLCE sheath layer, formed through shear-stress-based extrusion, also exhibited vivid reflective colours along with the black TPE core. We have further investigated the mechanochromic properties of fibers subjected to varying coating rates. The coating process was conducted at reduced rates of 10% (0.3 mm/s), 30% (0.9 mm/s), and 60% (1.8 mm/s) of the original speed (3 mm/s) (Supplementary Fig. 4). The results indicate no significant variations in mechanochromic behavior under the range of coating rates from 0.3 to 3 mm/s (Supplementary Fig. 4). Finally, UV irradiation at 365 nm was conducted to cross-link the CLCE precursor to lock in a thin layer of the helical structure (Stage IV). Differential scanning calorimetry (DSC) (Supplementary Fig. 5) revealed the glass transition temperature (T_g) of CLCE to be -10 °C, which confirms its rubbery state at room temperature.

The coating temperature was optimised on the basis of rheological studies because the viscoelasticity of the CLCE precursor determines the shear-induced arrangement of the cholesteric helix. The scanning electron microscopy (SEM) images of the fibres at 30 °C showed poor coating with CLCE-free regions, indicating that high elasticity in the cholesteric phase leads to poor wettability (Fig. 1d). In contrast, the uniform coating is attributed to the enhanced coating ability of CLCE above T_{IC} (Fig. 1e, f). In addition, the thickness uniformity analysis showed irregular thicknesses ranging from 0 to 65.5 µm at 30 °C, but above the T_{IC} (54 °C), the variation decreased, with average thicknesses of 14.98 ± 8.07 µm at 54 °C and 10.86 ± 5.24 µm at 80 °C (Supplementary Fig. 6). Although a uniform coating layer was achieved at 54 and 80 °C, the reflective colour was significantly more vivid at 54 °C than at 80 °C. The cloudy appearance is attributed to the absence of cholesteric order in the CLCE precursor within the isotropic phase (Fig. 1f). Although shear forces can temporarily induce paranematic alignment, they fail to establish the desired helical structure due to the absence of cholesteric order during the imposed shear at 80 °C. Consequently, during the cooling process as the isotropic phase of precursor transitions into the cholesteric phase, the absence of shear stress support leads to a relatively poor alignment of the helical structure, thereby resulting in diffuse reflection. Notably, the formation of the shear-induced structure was favourable at 54 °C. The rheological behavior of CLCE precursors and their viscoelastic impact on shear-induced helix alignment at various temperatures are detailed in Supplementary Note 3 and Supplementary Fig. 7. Furthermore, a detailed analysis of the mechanochromic performance of the CLCE-SC fibres as a function of coating thickness was conducted (Supplementary Fig. 8). The results showed that fibers with thicker coatings exhibited a broader initial reflection band. As the coating thickness increases, the effect of shear stress diminishes, resulting in reduced stress transmission to the inner layers, thus leading to poor alignment of the cholesteric helix. The results revealed that a coating thickness of 15 µm is optimal for forming a uniaxially aligned cholesteric helix, ensuring enhanced mechanochromic performance and uniformity.

The axis of the helical structure was radially aligned to the cross-section of the core fibre (Fig. 1g). Cross-sectional SEM images showed a well-coated CLCE sheath around the core fibre, revealing a helical structure with a helical pitch (p) of 613 nm in the initial red state

(enlarged SEM image in Fig. 1g). The wavelength of the reflected light from this helical structure can be expressed as follows:

$$\lambda = np \cos \theta \quad (1)$$

where λ is the central reflection wavelength of the Bragg reflective spectrum, n is the average refractive index of the CLCE sheath, p is the cholesteric pitch that indicates the distance over which the helical structure completes one full turn, and θ is the angle between the incident light and helical axis. As illustrated in Fig. 1h, stretching the fibres along the x-axis thinned the CLCE sheath, shortening the helical pitch and shifting the reflective wavelength from red to blue. The single CLCE-SC fibre clearly exhibited mechanochromic blueshift properties under different loads (200 g, 500 g, 1 kg) (Fig. 1i).

Toughness and low hysteresis of CLCE-SC fibres

Our composite fibre system can withstand significantly higher loads compared to traditional CLCE fibres or films, which would not be possible with conventional CLCE structures alone. To highlight the superiority of our system, a comparison with recent studies on CLCE is presented in Table S1. To demonstrate the significantly enhanced mechanical performance of our CLCE-SC fibres than that of the neat CLCE fibres, we conducted various mechanical analyses while applying engineering strain (ϵ) along the x-axis. The ultimate tensile strength of the CLCE-SC fibre (100.9 MPa) was more than eight times higher than that of the neat CLCE fibre (11.6 MPa) (Supplementary Fig. 9). Furthermore, the toughness of the CLCE-SC fibre (2.7×10^2 MJ m⁻³) was over 84 times higher than that of the neat CLCE fibre (3.2 MJ m⁻³), indicating significantly improved energy storage capacity due to the SC structure (Fig. 2a). The neat CLCE fibres exhibit high hysteresis owing to soft elasticity^{34,35} and require some time for mesogen reorientation upon stretching. The hysteresis loops of the neat CLCE and CLCE-SC fibres exhibited different recovery behaviours upon stretching with 65% strain (ϵ) (Fig. 2b); while the neat CLCE fibres demonstrated plastic recovery with high hysteresis, the CLCE-SC fibres showed elastic recovery with minimal hysteresis. Moreover, the neat CLCE fibres recovered up to 20% strain in this cyclic test, and the subsequent recovery progressed gradually because of slow reorientation. In contrast, the CLCE-SC fibres rapidly returned to their original state upon unloading, which was ascribed to the high elasticity and low hysteresis of TPE. This low hysteresis was maintained even after 10 cycles of repeated loops (Supplementary Fig. 10). Next, we estimated the tangent modulus⁴⁴⁻⁴⁶, which represents the elastic modulus of the material at each strain upon unloading (Fig. 2c). The neat CLCE fibres showed elastic recovery and a consistent decrease in the tangent modulus in the initial contraction section from 65% to 20% strain, at which point the tangent modulus became 0 MPa; this signifies a transition from elastic to plastic deformation. Conversely, the CLCE-SC fibres exhibited positive tangent modulus until the recovery was complete, indicating full elastic recovery. The inset graph reveals the differences in the tangent moduli of the two fibres.

The CLCE-SC fibres exhibited immediate response and rapid relaxation upon repeated mechanical stretching, even during ultra-fast loading-unloading cycles with up to 60% strain and upon increasing the frequency from 3.03 Hz ($= 18.18$ cm s⁻¹) to 8.33 Hz ($= 49.98$ cm s⁻¹) (Fig. 2d and Supplementary Movie 1). In contrast, the neat CLCE fibres underwent slow relaxation due to plastic deformation upon unloading at a strain of 60% ($\epsilon = 60\%$) and upon increasing the frequency from 3.03 Hz to 8.33 Hz (Fig. 2e and Supplementary Movie 2). To the best of our knowledge, such exceptional mechanochromic responsiveness has not been demonstrated in previous studies. This rapid response rate confirms that the CLCE-SC fibres can exhibit stable and reliable mechanochromic properties in highly dynamic, real-world environments. Notably, the relaxation speeds of the CLCE-SC and neat CLCE

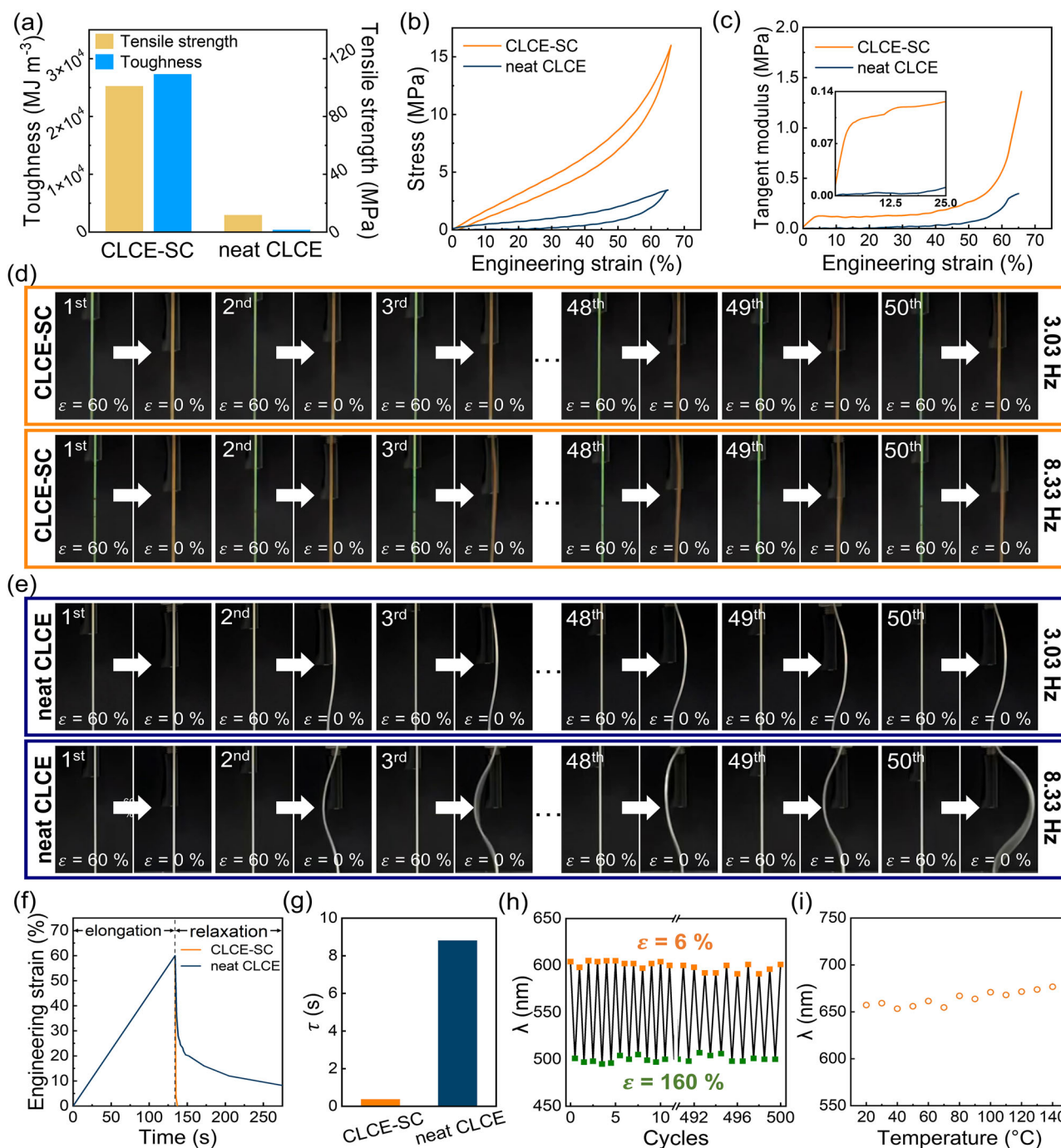


Fig. 2 | Mechanical properties and durability of the CLCE-SC and neat CLCE fibres. **a** Toughness and tensile strength of the CLCE-SC and neat CLCE fibres. **b** Hysteresis loops of the CLCE-SC and neat CLCE fibres elongated up to 65% strain. **c** Tangent moduli in the unloading stage of the hysteresis loop in (b). The inset shows the enlarged section of up to 25% strain. **d** and **e** Ultra-fast strain-relaxation cyclic tests of CLCE-SC and neat CLCE fibres up to 50 cycles at 3.03 and 8.33 Hz. The

CLCE-SC and neat CLCE fibres were elongated by 60% strain. **f** Creep recovery test over time after a constant elongation speed (0.011 cm s^{-1}) up to 60% strain. **g** Relaxation time (τ) of the CLCE-SC and neat CLCE fibres. **h** Reflective wavelength of the CLCE-SC fibres during strain-relaxation tests up to 500 cycles, ranging from 6 to 160% strain. **i** Thermal stability test of the CLCE-SC fibres at increasing temperatures up to 140 $^{\circ}\text{C}$.

fibres were completely different. Therefore, we conducted a creep recovery test to quantitatively estimate the time required for complete recovery (Fig. 2f and Supplementary Fig. 11a). The CLCE-SC fibres recovered within 0.4 s upon elongation to 60% strain ($\epsilon = 60\%$) at a strain speed of 0.011 cm s^{-1} and subsequent release. In contrast, the neat CLCE fibres recovered from 60% to 20% strain within 17.4 s, following which the relaxation speed significantly slowed, requiring

1,380 s for complete recovery. These results are consistent with the convergence of the tangent modulus to 0 MPa from 20% strain (Fig. 2c). To quantitatively compare the relaxation behaviour of these fibres from a viscoelastic perspective, we determined their relaxation time (τ)^{47,48}; τ is defined as the rate at which a material recovers its initial strain after deformation. The decrease in the strain over time after the removal of the applied stress can be described by the

Kelvin–Voigt model creep test equation.

$$\varepsilon(t) = \varepsilon_0 \exp\left(-\frac{t}{\tau}\right) \quad (2)$$

where ε_0 is the initial strain at the point of stress removal, t is the time, and τ is the relaxation time. τ can be expressed as

$$\tau = \frac{\eta}{E} \quad (3)$$

where η is the viscosity coefficient and E is the elastic modulus of the material, and higher elasticity corresponds to lower τ . The CLCE-SC fibres exhibited a low τ (0.37 s) owing to the high elasticity of the core TPE fibre (Fig. 2g and Supplementary Fig. 11b). In contrast, the neat CLCE fibres exhibited ~24 times higher τ (8.81 s), owing to their considerably lower elasticity than that of the CLCE-SC fibre.

Additionally, to assess the mechanical durability of the CLCE-SC fibres, we subjected them to 500 cycles of tensile strain relaxation at up to 160% strain ($\varepsilon = 160\%$). The shift in reflective wavelength was stable during all cycles (Fig. 2h). We also examined the thermal stability of the fibres by monitoring the reflective colours at different temperatures. The reflective colour of the CLCE sheath remained stable up to 140 °C (Fig. 2i and Supplementary Fig. 12).

Tuneable mechanochromic properties of CLCE-SC fibres

The tuneability of mechanochromism across a broad range is essential for its application in diverse real-world environments. Here, the elasticity of the CLCE-SC fibres can be tuned by simply adjusting the properties of the TPE core with different amount of CB filler, which was chosen for its superior compatibility⁴⁹ and processability⁵⁰ compared to other black fillers, such as carbon nanotubes (CNTs)⁵¹ and graphene oxide (GO)⁵². Furthermore, by implementing a black core substrate, the reflective colours of the CLCE sheath were further enhanced, achieving greater contrast and vibrancy in the mechanochromic response (Supplementary Fig. 13). To explore the effect of varying elastic modulus, three types of CLCE-SC fibres were synthesised: low modulus (LM)-, medium modulus (MM)-, and high modulus (HM)-CLCE-SC fibres. Their mechanical and optical properties were investigated. The Young's moduli of the LM-, MM-, and HM-CLCE-SC fibres were 11, 18, and 23 MPa, respectively (Fig. 3a), which are 22–46 times higher than that of the neat CLCE fibres (0.5 MPa)³¹. Although the mechanical behaviour of the CLCE-SC fibres reflects that of the neat TPE core fibres (Supplementary Fig. 14), microcracks appeared on the surface of the CLCE-SC fibres at strains exceeding 170%. However, within the strain range of up to 170%, such as at 100% strain, the fibres maintained a stable surface even after 100 cycles of repeated deformation (Supplementary Fig. 15 and Supplementary Movie 3). Additionally, even at deformation levels exceed 170%, such as at 200% strain, although microcracks occur, it has been observed that the mechanochromic performance remains stable with the corresponding peak shift (Supplementary Fig. 16). The maximum stress values for the HM-, MM-, and LM-CLCE-SC fibres at 170% strain ($\varepsilon = 170\%$) were 41.1, 27.3, and 15.8 MPa, respectively, which are approximately twice as high as that of the neat CLCE fibres (~8 MPa)³¹. This demonstrates the tuneable mechanical properties of the CLCE-SC fibres. Furthermore, the similar Poisson's ratios for LM-, MM-, and HM-CLCE-SC fibres indicate consistent adhesion of the CLCE sheath to the TPE fibres, regardless of CB content (Supplementary Fig. 17 and see the description regarding Poisson's effect in Supplementary Note 4). In addition, we demonstrated on-demand initial reflective colours by varying concentrations of chiral dopant LC 756 (Fig. 3b and Supplementary Table 2). The CLCE-SC fibres with different λ_0 values successfully demonstrated mechanochromic performance at 50% strain (Fig. 3c). Additionally, the fibres showed intense selective reflection because of

the black colour of the TPE core. This TPE core was clearly visible against any background from black to white, whereas the neat CLCE fibres were hardly visible against brighter backgrounds (Fig. 3d).

The strain- or stress-dependent colour palettes of the CLCE-SC fibres up to 170% strain and 6 N load were obtained (Fig. 3e–g and Supplementary Fig. 18). As the strain increased, the reflective colour shifted from red to blue, which was consistent across all modulus conditions. At the same strain, the CLCE sheath exhibited reflective colours similar to those of the LM-, MM-, and HM-CLCE-SC fibres (Fig. 3e). The LM-, MM-, and HM-CLCE-SC fibres exhibited peaks at 529, 540, and 542 nm, respectively, at 80% strain and 492, 497, and 495 nm, respectively, at 170% strain (Fig. 3f). We also investigated the mechanochromic blue shift of the LM-, MM-, and HM-CLCE-SC fibres under the same load from 0 to 6 N (Fig. 3g). Their reflection shifts differed significantly. The higher the elastic modulus, the lower the degree of tensile strain under the same load. At an applied load of 6 N, the LM-, MM-, and HM-CLCE-SC fibres exhibited 200%, 100%, and 60% strains, respectively, showing wavelengths of 489, 521, and 574 nm, respectively (Fig. 3h). Upon further loading, the LM-, MM-, and HM-CLCE-SC fibres exhibited reflective colour shifts to blue, green, and deep yellow, respectively. In addition, fitting curves of the wavelengths revealed that all three types of fibres showed good agreement with the reflective colour shifts by strain and stress (Fig. 3f–h) (see the details regarding fitting curves in Fig. 3f and h in Supplementary Note 5). Our CLCE-SC fibres show distinct reflective colours under varying loads and strains, with LM fibres as high-sensitivity indicators for subtle stress variations and HM fibres as low-sensitivity indicators for broader stress ranges.

Application of CLCE-SC fibres for real-world stress detection

We evaluated the performance of our CLCE-SC fibres as smart fishing lines, bundled safety ropes, and a two-dimensional mechanochromic textile called a dynamic sensory net. To demonstrate the applicability of the fibres as smart fishing lines, three fish toys of 200, 500, and 800 g were loaded on a single, red MM-CLCE-SC fibre ($\lambda_0 = 673$ nm) (Fig. 4a); the reflective colour shifted from orange to blue as the weight increased. These smart fishing lines can be used to predict the size of fish before lifting them out of the water, leading to more effective fishing. To demonstrate the applicability of the fibres as bundled safety ropes, we twisted seven strands of the red HM-CLCE-SC fibres to create a rope. This rope changes colour as each strand is sequentially severed, indicating its safety status. The rope turned green when a 5 kg kettlebell was suspended from it (Fig. 4b). As each strand was sequentially severed from seven to three, the rope changed colour from green to blue, which is a direct indication of the tension exerted upon them. This colour change was clearly visible to the naked eye, confirming its potential of the fibres as a safety rope. Smart safety ropes capable of supporting a person can be manufactured using a sufficient number of the CLCE-SC fibres and a suitable twisting pattern. Finally, a net-like textile called a dynamic sensory net was prepared by interweaving nine LM-CLCE-SC fibre strands horizontally and vertically within a square frame (Fig. 4c). The net exhibited immediate mechanochromic responses even under ultra-fast and strong deformations, changing colour in real-time dynamic environments such as object collisions. When a 510 g steel ball was dropped onto the net from a height of 15 cm, the net changed colour. The steel ball caused significant stress and strain in the fibres, resulting in a proportional blue shift and recovery to its initial state within 1 s (side and bottom views in Fig. 4d–e). Additionally, we investigated the variation in the force exerted on the fibres of the dynamic sensory net depending on the height from which the steel ball was dropped (Fig. 4f and Supplementary Movie 4). The energy transmitted to the net varies with the potential energy of the steel ball, which depends on the initial drop height. The height was adjusted from 0.05 to 0.2 m in increments of 0.05 m. As the height increased, the potential energy increased from

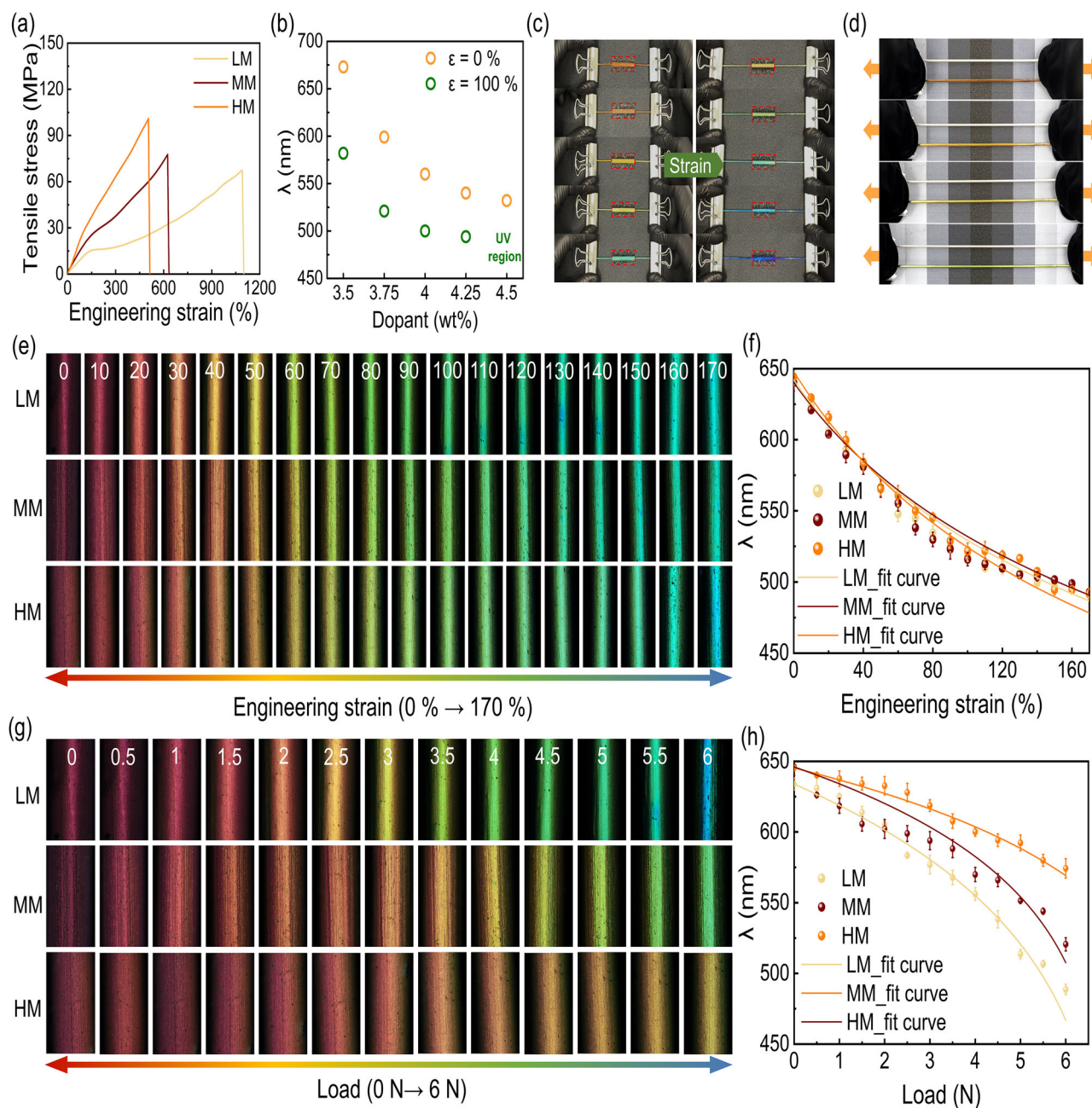


Fig. 3 | Mechanochromic properties of the CLCE-SC fibres. **a** Tensile stress–strain curves of the low modulus (LM)-, medium modulus (MM)-, and high modulus (HM)-CLCE-SC fibres. **b** Variation in the reflected wavelengths with different chiral dopant concentrations at 100% strain. **c** Photographs of the variation in the initial colours exhibited by the fibres at different dopant concentrations and their mechanochromic colour changes at 50% strain. Inset images within red dashed boxes

provide a magnified view of the fiber centers. **d** Comparison of the LM-CLCE-SC and neat CLCE fibres under various background brightness levels. **e** and **g** POM images showing the colour palettes for the LM-, MM-, and HM-CLCE-SC fibres under 170% strain and 6 N load. **f** and **h** Variation in the wavelengths with fitting curves for the LM-, MM-, and HM-CLCE-SC fibres under 170% strain and 6 N load.

0.25 to 1.00 J. This increased the stored energy of the net owing to the internal stress during the collision between the net and steel ball, broadening the colour-change region. Figure 4g shows a CIE chromaticity diagram of our mechanochromic sensor, demonstrating their on-demand broad range of colour shifts caused by different applied weights, number of fibre strands, and transferred energy.

Discussion

We developed ultra-tough and high-resilience mechanochromic fibres with a CLCE sheath and TPE core, enabling scalable and continuous production. Optimal sheath-core structure, uniform coating, and vivid

coloration were achieved at temperatures near the T_{IC} of the CLCE precursor. We produced fibres with varying moduli (LM, MM, HM) to control mechanical and optical properties on demand. Leveraging TPE strength, we achieved rapid strain relaxation (60% at 8.33 Hz), high strength (100.9 MPa), and toughness ($2.7 \times 10^2 \text{ MJ m}^{-3}$), meeting industrial needs. Our CLCE-SC mechanochromic fibres provide both functionality and aesthetic appeal, suitable for smart apparel and interior furnishings. As illustrated in Fig. 5, their ability to detect critical changes and trigger early warnings also makes them highly applicable in healthcare and aerodynamics, highlighting their strong potential as advanced responsive materials across various industries.

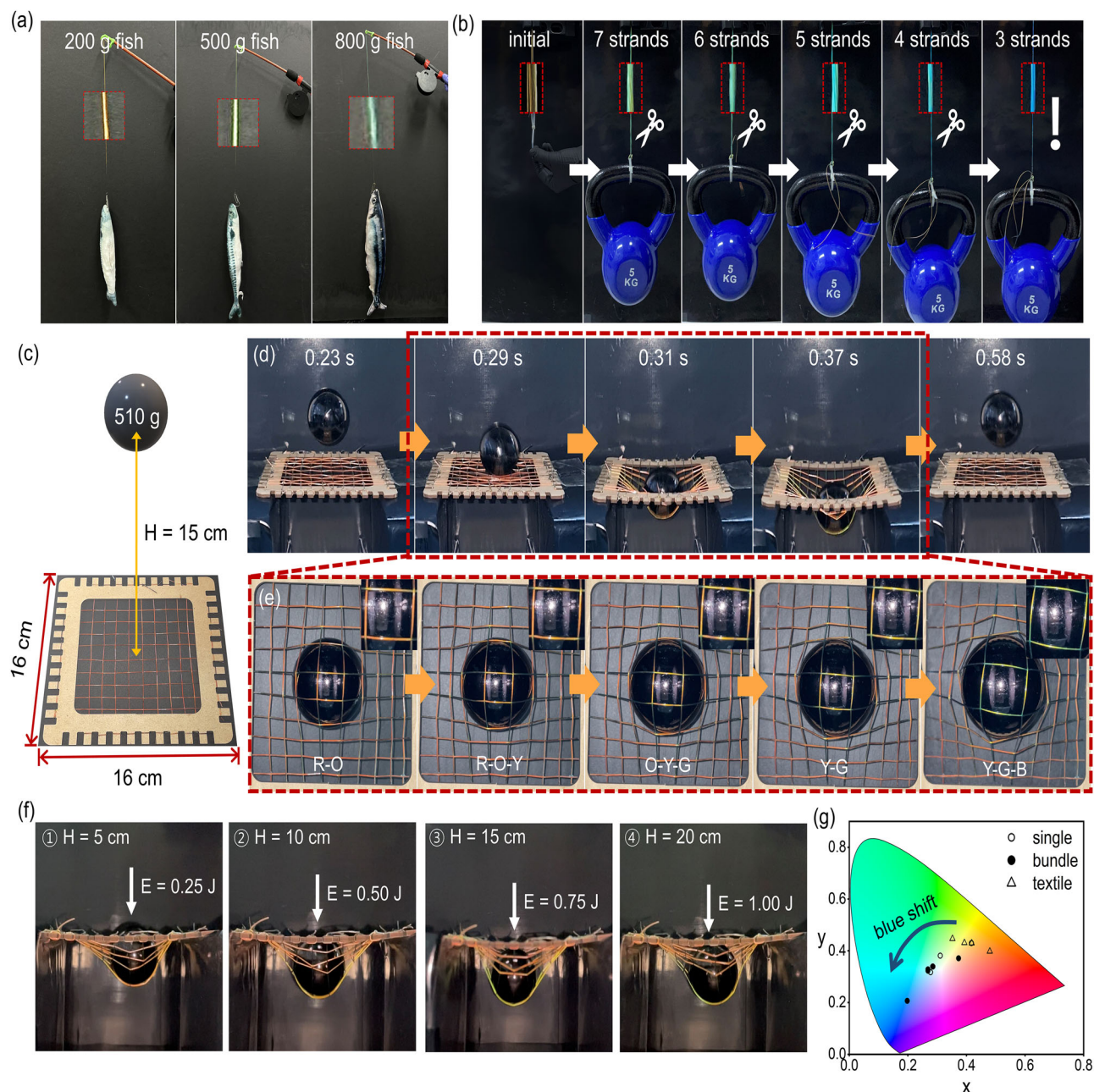


Fig. 4 | Mechanochromic applications of the CLCE-SC fibres. **a** Smart fishing lines fabricated from a single LM-CLCE-SC fibre loaded with three fish toys of 200, 500, and 800 g. **b** Bundled safety rope composed of seven strands of the HM-CLCE-SC fibres, supporting a 5 kg kettlebell. Sequential cutting of the seven strands to three. **c** Schematic of a dynamic sensory net interwoven with 9×9 strands of the LM-CLCE-SC fibres, tested by vertically dropping a steel ball from a height of 15 cm.

d and **e** Photographs of the side and bottom views of the dynamic sensory net during steel-ball dropping. The enlarged photos in **(e)** show the colour change from red (R) to orange (O), yellow (Y), green (G), and blue (B) at the centre of the net owing to the force applied by the steel ball. **f** Photographs of the deformed dynamic sensory net affected by different dropping heights and potential energies. **g** CIE chromaticity diagram for various applications.

Methods

Materials

Thermoplastic polyurethane (TPU, 1185 A 10) was purchased from BASF (Korea). Carbon black (CB, HI-black 50LB) was purchased from Info Chems (Korea). 1,5-pentanedithiol (>99%, 1,5-PDT), 2,2-dimethoxy-2-phenylacetophenone (DMPA), 1,8-diazabicyclo [5.4.0] undec-7-ene (98%, DBU), poly(vinyl alcohol) (PVA, Mw 31,000–50,000, 98–99% hydrolyzed) were purchased from Sigma Aldrich. Butylated hydroxytoluene (analytical standard, BHT) was purchased from Tokyo Chemical Industry Co. Hydrochloric acid (HCl, 36.5% to 38.0%) was purchased from Duksan Pure Chemical Co. Magnesium sulfate (MgSO_4 , anhydrous powder), dichloromethane (DCM), and ethanol

were purchased from Samchun Chemicals KOR. 2-methyl-1,4-phenylene bis(4-((6-(acryloyloxy)hexyl)oxy)benzoate) (RM82), 2-methyl-1,4-phenylene bis(4-((3-(acryloyloxy)propoxy)benzoate) (RM257), Chiral dopant (3 R,3aR,6S,6aR)-hexahydrofuro[3,2-b] furan-3,6-diyl bis(4-((4-((4-(acryloyloxy)butoxy) carbonyl)oxy) benzoyl)oxy)benzoate) (Paliocolor LC756) was purchased from Henan Wentao Chemical Product Co., Polydimethylsiloxane (PDMS) was purchased from Dowhitech Co.

Preparation of TPE/CB nanocomposite fibres

In order to remove moisture, TPE pellets and CB powder were dried in a vacuum oven at 60 °C overnight. TPE/CB composites were prepared

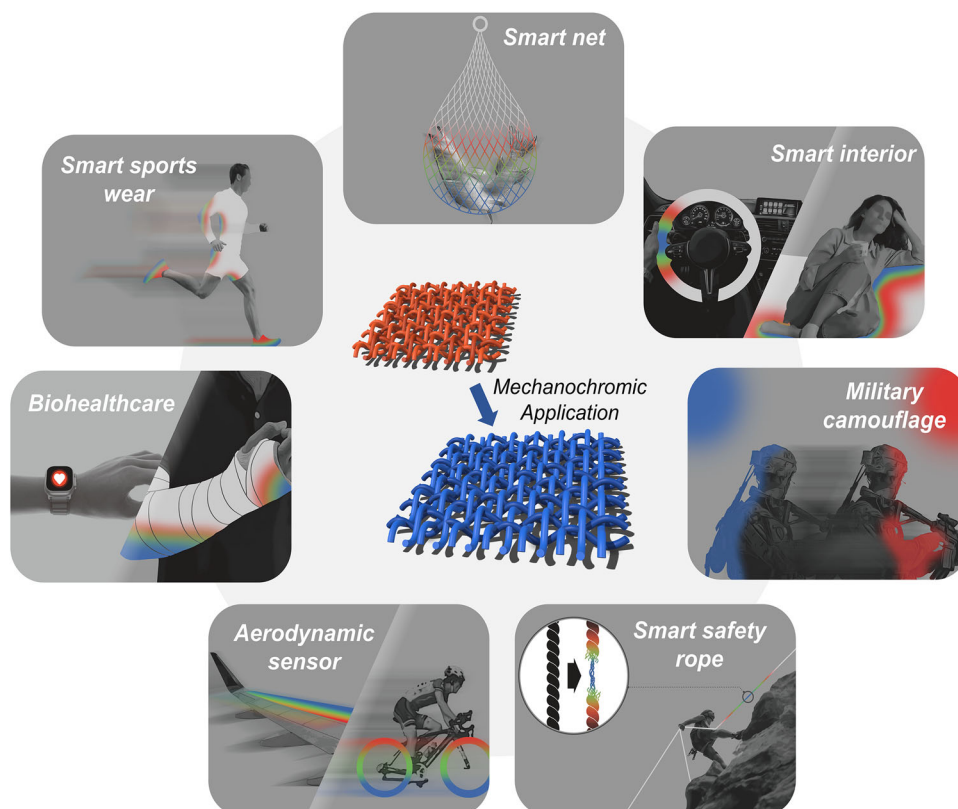


Fig. 5 | Potential applications of our CLCE-SC mechanochromic fibres in smart textile industries.

by shaking CB powder with TPE pellets. The concentrations of CB ranged from 0.08 to 2 wt% with respect to the TPE weight. The TPE/CB nanocomposite fibres were prepared using a lab-scale melt spinning system. Single screw extruder was maintained at 170 °C. The nanocomposite was extruded through one-hole spinneret (diameter: 2.8 mm) and subsequently cooled in the air. The fibres were collected with rotation speed of 3.0 m min⁻¹.

Preparation of LC oligomer

10 g reactive monomer, RM 82, were added into 80 ml dichloromethane (DCM) with rigorous stirring. 3 ml of 1,5 PDT as chain extender and four drops of DBU as catalyst were added into the solution. The reaction mixture was stirred at room temperature overnight. Subsequently, the mixture was washed with diluted HCl aqueous solution and diluted NaCl aqueous solution to remove unreacted monomer. After then, anhydrous MgSO₄ power was used to dry the solution for 20 min, followed by filtration. The resulting LC oligomer was obtained as viscous liquid after evaporating the solvent under vacuum.

Preparation of CLCE precursor

The photopolymerizable precursors were prepared by mixing a 66 wt% LC oligomer, 16 wt% RM 82 and RM 257 as a reactive monomer, 2 wt% DMPA as a photo-initiator, and 1 wt% BHT as an inhibitor for thermal polymerization. LC 756 as the chiral dopant was added from 3.5 wt% (red) to 4.5 wt% (blue). The mixture was vigorously mixed at 100 °C for 30 min.

Preparation of CLCE-SC fibres

Before coating the CLCE precursor as the sheath part on the core fibres, a plasma treatment was conducted on the core surface to introduce plenty of -OH groups, thereby increasing the coat-ability of the CLCE precursor. The TPE fibres passed through the PDMS chamber

containing the CLCE precursor, which is maintained at 60 °C. The fibres then passed through a conical chamber slightly larger than the fibre diameter (0.9 mm), where the mesogens experienced shear to form a uniaxially oriented cholesteric phase. The CLCE-SC fibres were obtained through UV-induced crosslinking immediately after coating.

Preparation of neat CLCE fibres

Round capillaries were coated with 1 wt% PVA aqueous solution, and then baked at 120 °C for 1 h. After then, the CLCE precursor was soaked up into the capillary by vacuum pump and polymerized using 365 nm UV light. The neat CLCE fibres were obtained by breaking the glass capillary after dissolving the PVA layer through soaking in deionized water.

Characterization

The mechanical properties of fibres were measured using a universal testing machine (RB 302 Microload, R&B Inc., Korea) loaded with a 10 kgf load cell. The specimens were cut to length of 8 cm and gage length was 2 cm. Tensile test was conducted at crosshead speed of 100 mm min⁻¹. In hysteresis test, the specimens were stretched up to a strain of 65% or 95% and then release immediately. The crosshead speed was 10 mm min⁻¹. The loading-unloading cyclic test was conducted using elongation-relaxation cyclic equipment operating at multiple frequency levels (Daesan Scientific Co., Korea). The specimens were cut to length of 10 cm and gage length was 5 cm. The glass transition temperatures (*T_g*) of CLCE precursor were measured using a differential scanning calorimetry (DSC, Diamo, Perkin Elmer). Samples were placed on aluminum hermetic crucibles and scanned at two cycles of cooling and heating from -30 to 70 °C with a rate of 20 °C min⁻¹. Optical microscope and polarized optical microscope (LV100POL, Nikon, Japan) was employed to observe the CLCE-SC fibres. Spectrometer (DS-F13, Nikon, Japan) was used to determine the wavelength shift corresponding to mechanical deformation. The

surface morphology and nanostructure of CLCE sheath layer were analyzed using a Scanning electron microscope (MIRA3 LMH, Tescan). Plasma cleaner (PDC-32G-2, Harrick Plasma) was utilized to introduce hydroxy groups onto the TPE core surface. The rheological properties of liquid crystal solutions were evaluated using a rotational rheometer (MCR 302e, Anton Paar, Austria) with a concentric cylinder geometry. Dynamic frequency sweeps were conducted in an angular frequency range of 0.5–500 rad s⁻¹. Temperature ranged from 30 to 80 °C with intervals of 10 °C and shear strain was 5%, respectively. Temperature sweeps were conducted by heating the solution from 30 to 80 °C. The measurements were performed at shear strain of 5% and angular frequency of 1 rad s⁻¹. In stress sweeps, shear stress was varied from 0.1 to 1000 Pa and angular frequency was 1 rad s⁻¹. Temperature ranged from 30 to 80 °C with intervals of 10 °C.

Data availability

The authors declare that the data supporting the findings of this study are available within the paper and its supplementary information files. Data is also available from the authors on request.

References

- Zhao, X. et al. Smart Ti₃C₂T_x MXene fabric with fast humidity response and joule heating for healthcare and medical therapy applications. *ACS Nano* **14**, 8793–8805 (2020).
- Tat, T. et al. Smart textiles for healthcare and sustainability. *ACS Nano* **16**, 13301–13313 (2022).
- Liu, X. et al. Smart textile based on 3D stretchable silver nanowires/mxene conductive networks for personal healthcare and thermal management. *ACS Appl. Mater. Interfaces* **13**, 56607–56619 (2021).
- Issatayeva, A., Beisenova, A., Tosi, D. & Molardi, C. Fiber-optic based smart textiles for real-time monitoring of breathing rate. *Sensors* **20**, 3408 (2020).
- Tamayol, A. et al. Flexible pH-sensing hydrogel fibers for epidermal applications. *Adv. Healthc. Mater.* **5**, 711–719 (2016).
- He, H. et al. An ultralight self-powered fire alarm e-textile based on conductive aerogel fiber with repeatable temperature monitoring performance used in firefighting clothing. *ACS Nano* **16**, 2953–2967 (2022).
- Li, J. et al. A new type of optical fiber glucose biosensor with enzyme immobilized by electrospinning. *IEEE Sens. J.* **21**, 16078–16085 (2021).
- Zhao, Y. et al. Highly stretchable and strain-insensitive fiber-based wearable electrochemical biosensor to monitor glucose in the sweat. *Anal. Chem.* **91**, 6569–6576 (2019).
- Lee, S. et al. Ag nanowire reinforced highly stretchable conductive fibers for wearable electronics. *Adv. Funct. Mater.* **25**, 3114–3121 (2015).
- Li, L. et al. Ultrastretchable fiber sensor with high sensitivity in whole workable range for wearable electronics and implantable medicine. *Adv. Sci.* **5**, 1800558 (2018).
- Leal-Junior, A., Avellar, L., Frizera, A. & Marques, C. Smart textiles for multimodal wearable sensing using highly stretchable multiplexed optical fiber system. *Sci. Rep.* **10**, 13867 (2020).
- Wen, Z. et al. Self-powered textile for wearable electronics by hybridizing fiber-shaped nanogenerators, solar cells, and supercapacitors. *Sci. Adv.* **2**, e1600097 (2016).
- Chen, G. & Hong, W. Mechanochromism of structural-colored materials. *Adv. Optical Mater.* **8**, 2000984 (2020).
- Clough, J. M., Weder, C. & Schrettl, S. Mechanochromism in structurally colored polymeric materials. *Macromol. Rapid Commun.* **42**, 2000528 (2021).
- Guan, Y., Li, H., Zhang, S. & Niu, W. Mechanochromic photonic vitrimer thermal management device based on dynamic covalent bond. *Adv. Funct. Mater.* **33**, 2215055 (2023).
- Wang, X. et al. Polystyrene@poly(methyl methacrylate-butyl acrylate) core-shell nanoparticles for fabricating multifunctional photonic crystal films as mechanochromic and solvatochromic sensors. *ACS Appl. Nano Mater.* **5**, 729–736 (2022).
- Guo, Q. & Zhang, X. A review of mechanochromic polymers and composites: from material design strategy to advanced electronics application. *Compos. Part B: Eng.* **227**, 109434 (2021).
- Li, H., Sun, X. & Peng, H. Mechanochromic fibers with structural color. *ChemPhysChem* **16**, 3761–3768 (2015).
- Colaco, R. et al. Mechanochromic microfibers stabilized by polymer blending. *ACS Appl. Polym. Mater.* **2**, 2055–2062 (2020).
- Sandt, J. D. et al. Stretchable optomechanical fiber sensors for pressure determination in compressive medical textiles. *Adv. Healthc. Mater.* **7**, 1800293 (2018).
- Kim, J. H. et al. Microfluidic production of mechanochromic photonic fibers containing nonclose-packed colloidal arrays. *Small Sci.* **1**, 2000058 (2021).
- Zhao, R., He, Y., He, Y. & Hou, C. Mechanochromic photonic fibers composed of strain responsive colloidal crystals and spandex yarns. *Colloids Surf. A: Physicochemical Eng. Asp.* **671**, 131689 (2023).
- Sun, X., Zhang, J., Lu, X., Fang, X. & Peng, H. Mechanochromic photonic-crystal fibers based on continuous sheets of aligned carbon nanotubes. *Angew. Chem. Int. Ed.* **54**, 3630–3634 (2015).
- Zhang, J. et al. The continuous fabrication of mechanochromic fibers. *J. Mater. Chem. C* **4**, 2127–2133 (2016).
- Zhao, R. et al. Dual-mode fiber strain sensor based on mechanochromic photonic crystal and transparent conductive elastomer for human motion detection. *ACS Appl. Mater. Interfaces* **15**, 16063–16071 (2023).
- Kim, D.-Y., Lee, K. M., White, T. J. & Jeong, K.-U. Cholesteric liquid crystal paints: in situ photopolymerization of helicoidally stacked multilayer nanostructures for flexible broadband mirrors. *NPG Asia Mater.* **10**, 1061–1068 (2018).
- Kizhakidathazhath, R. et al. Facile anisotropic deswelling method for realizing large-area cholesteric liquid crystal elastomers with uniform structural color and broad-range mechanochromic response. *Adv. Funct. Mater.* **30**, 1909537 (2020).
- Choi, J. et al. Direct-ink-written cholesteric liquid crystal elastomer with programmable mechanochromic response. *Advanced Functional Materials*, **34**, 2310658 (2023).
- Han, W. C. et al. Versatile mechanochromic sensor based on highly stretchable chiral liquid crystalline elastomer. *Small* **19**, 2206299 (2023).
- Kim, S.-U. et al. Broadband and pixelated camouflage in inflating chiral nematic liquid crystalline elastomers. *Nat. Mater.* **21**, 41–46 (2022).
- Geng, Y., Kizhakidathazhath, R. & Lagerwall, J. P. F. Robust cholesteric liquid crystal elastomer fibres for mechanochromic textiles. *Nat. Mater.* **21**, 1441–1447 (2022).
- Geng, Y. & Lagerwall, J. P. F. Multiresponsive cylindrically symmetric cholesteric liquid crystal elastomer fibers templated by tubular confinement. *Adv. Sci.* **10**, 2301414 (2023).
- Warner, M., Bladon, P. & Terentjev, E. M. Soft elasticity” — deformation without resistance in liquid crystal elastomers. *J. Phys. II Fr.* **4**, 93–102 (1994).
- Merkel, D. R., Shaha, R. K., Yakacki, C. M. & Frick, C. P. Mechanical energy dissipation in polydomain nematic liquid crystal elastomers in response to oscillating loading. *Polymer* **166**, 148–154 (2019).
- Azoug, A. et al. Viscoelasticity of the polydomain-monodomain transition in main-chain liquid crystal elastomers. *Polymer* **98**, 165–171 (2016).
- Lee, K. et al. Stress-strain behavior of the electrospun thermoplastic polyurethane elastomer fiber mats. *Macromol. Res.* **13**, 441–445 (2005).

37. Wang, X. et al. A highly stretchable carbon nanotubes/thermo-plastic polyurethane fiber-shaped strain sensor with porous structure for human motion monitoring. *Compos. Sci. Technol.* **168**, 126–132 (2018).
38. Zhang, S. et al. High conductive free-written thermoplastic polyurethane composite fibers utilized as weight-strain sensors. *Compos. Sci. Technol.* **189**, 108011 (2020).
39. Seyedin, S., Razal, J. M., Innis, P. C., Jalili, R. & Wallace, G. G. Compositional effects of large graphene oxide sheets on the spinnability and properties of polyurethane composite fibers. *Adv. Mater. Inter* **3**, 1500672 (2016).
40. Ma, R., Kang, B., Cho, S., Choi, M. & Baik, S. Extraordinarily high conductivity of stretchable fibers of polyurethane and silver nano-flowers. *ACS Nano* **9**, 10876–10886 (2015).
41. Picot, O. T., Dai, M., Broer, D. J., Peijs, T. & Bastiaansen, C. W. M. New approach toward reflective films and fibers using cholesteric liquid-crystal coatings. *ACS Appl. Mater. Interfaces* **5**, 7117–7121 (2013).
42. Yue, X. et al. Highly stretchable and durable fiber-shaped strain sensor with porous core-sheath structure for human motion monitoring. *Compos. Sci. Technol.* **189**, 108038 (2020).
43. Emeršić, T. et al. Stable non-equilibrium structures in chiral nematics under microfluidic flow. *J. Phys. Chem. B* **128**, 11441–11449 (2024).
44. Li, L. Characterization of multi-step cyclic-fatigue hysteresis behavior of 2D SiC/SiC composite using inverse tangent modulus. *Ceram. Int.* **50**, 4392–4403 (2024).
45. Guo, X. et al. Design, fabrication, and testing of CVI-SiC/SiC turbine blisk under different load spectrums at elevated temperature. *High. Temp. Mater. Process.* **41**, 279–288 (2022).
46. Kumar, R., Mikkelsen, L. P., Lilholt, H. & Madsen, B. Weibull parameters determined from a comprehensive dataset of tensile testing of single carbon fibres. *Data Brief.* **55**, 110717 (2024).
47. Xie, Y., Hill, C. A. S., Jalaludin, Z. & Sun, D. The water vapour sorption behaviour of three celluloses: analysis using parallel exponential kinetics and interpretation using the Kelvin-Voigt viscoelastic model. *Cellulose* **18**, 517–530 (2011).
48. Barnes, H. A. *An introduction to rheology* (pp. 11–36). Elsevier Science Ltd (1989).
49. Tang, H., Chen, X. & Luo, Y. Electrical and dynamic mechanical behavior of carbon black filled polymer composites. *Eur. Polym. J.* **32**, 963–966 (1996).
50. Athreya, S. R., Kalaitzidou, K. & Das, S. Mechanical and micro-structural properties of Nylon-12/carbon black composites: Selective laser sintering versus melt compounding and injection molding. *Compos. Sci. Technol.* **71**, 506–510 (2011).
51. Gahlout, P. & Choudhary, V. EMI shielding response of polypyrrole-MWCNT/polyurethane composites. *Synth. Met.* **266**, 116414 (2020).
52. He, L. & Tjong, S. C. Low percolation threshold of graphene/polymer composites prepared by solvothermal reduction of graphene oxide in the polymer solution. *Nanoscale Res Lett.* **8**, 132 (2013).

Acknowledgements

This work was supported by the National Research Foundation of Korea (NRF) grant funded by the Korea government (MSIT) (RS-2024-00457165).

(D.S.K.) This work was supported by the Nano & Material Development Program through the National Research Foundation of Korea funded by Ministry of Science and ICT (RS-2024-00408845). (Y.E.).

Author contributions

Y.J.J.: Writing–review & editing, Writing–original draft, Methodology, Formal analysis, Data curation. Y.L.: Writing–review & editing, Visualization, Methodology, Formal analysis, Data curation. T.W.: Methodology. J.L.: Methodology. Y.E.: Validation, Supervision, Resources, Writing–original draft, Writing–review & editing. D.S.K.: Validation, Supervision, Resources, Project administration, Writing–original draft, Writing–review & editing. Y.J.J. and Y.L. are equally contributed to this work.

Competing interests

The authors declare no competing interests.

Additional information

Supplementary information The online version contains supplementary material available at <https://doi.org/10.1038/s41467-025-57522-1>.

Correspondence and requests for materials should be addressed to Youngho Eom or Dae Seok Kim.

Peer review information *Nature Communications* thanks Jan Lagerwall and the other, anonymous, reviewers for their contribution to the peer review of this work. A peer review file is available.

Reprints and permissions information is available at <http://www.nature.com/reprints>

Publisher's note Springer Nature remains neutral with regard to jurisdictional claims in published maps and institutional affiliations.

Open Access This article is licensed under a Creative Commons Attribution-NonCommercial-NoDerivatives 4.0 International License, which permits any non-commercial use, sharing, distribution and reproduction in any medium or format, as long as you give appropriate credit to the original author(s) and the source, provide a link to the Creative Commons licence, and indicate if you modified the licensed material. You do not have permission under this licence to share adapted material derived from this article or parts of it. The images or other third party material in this article are included in the article's Creative Commons licence, unless indicated otherwise in a credit line to the material. If material is not included in the article's Creative Commons licence and your intended use is not permitted by statutory regulation or exceeds the permitted use, you will need to obtain permission directly from the copyright holder. To view a copy of this licence, visit <http://creativecommons.org/licenses/by-nc-nd/4.0/>.

© The Author(s) 2025